Supporting Information

Localized Permeabilization of E. coli Membranes by the Antimicrobial Peptide Cecropin A

Nambirajan Rangarajan, Somenath Bakshi, and James C. Weisshaar

Axial and transverse intensity profiles

To generate an axial intensity profile (or axial linescan) in ImageJ, fluorescence intensity was integrated for all the pixels along the short cell axis *y* at each *x* and plotted against *x*. See Fig. 7.

To generate a transverse intensity profile (Fig. S1), a line segment of variable width was drawn along the short, *y* axis of the cell. For each *y* value, fluorescence intensity was integrated for all *x* values within the width of the segment drawn. The transverse profile of the initial periplasmic GFP distribution has two peaks corresponding to the projection onto the *xy* plane of the shell of fluorescence from the periplasmic GFP (Fig. S1). The dip between the peaks is primarily due to periplasmic GFP at the top and bottom of the cell, plus fluorescence from GFP molecules that remain in the cytoplasm and some cell autofluorescence.

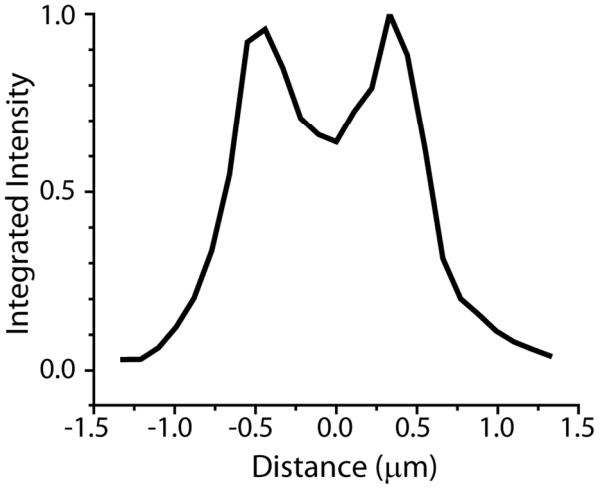

Figure S1. Transverse intensity linescan of the periplasmic GFP fluorescence prior to membrane permeabilization.

Relative axial coordinate of permeabilization events

To place locations of OM and CM permeabilization events for different cells on a common relative axial scale, we form an axial linescan (along the long axis *x*) for an image just prior to OM permeabilization. The two pixels closest to the full width at half-maximum height (FWHM) points were defined as the locations of $x_{rel} = 0$ and 1. In non-septating cells, $x_{rel} = 0$ was assigned to the cell tip near which GFP loss began. In septating cells, the assignment of $x_{rel} = 0$ was arbitrary.

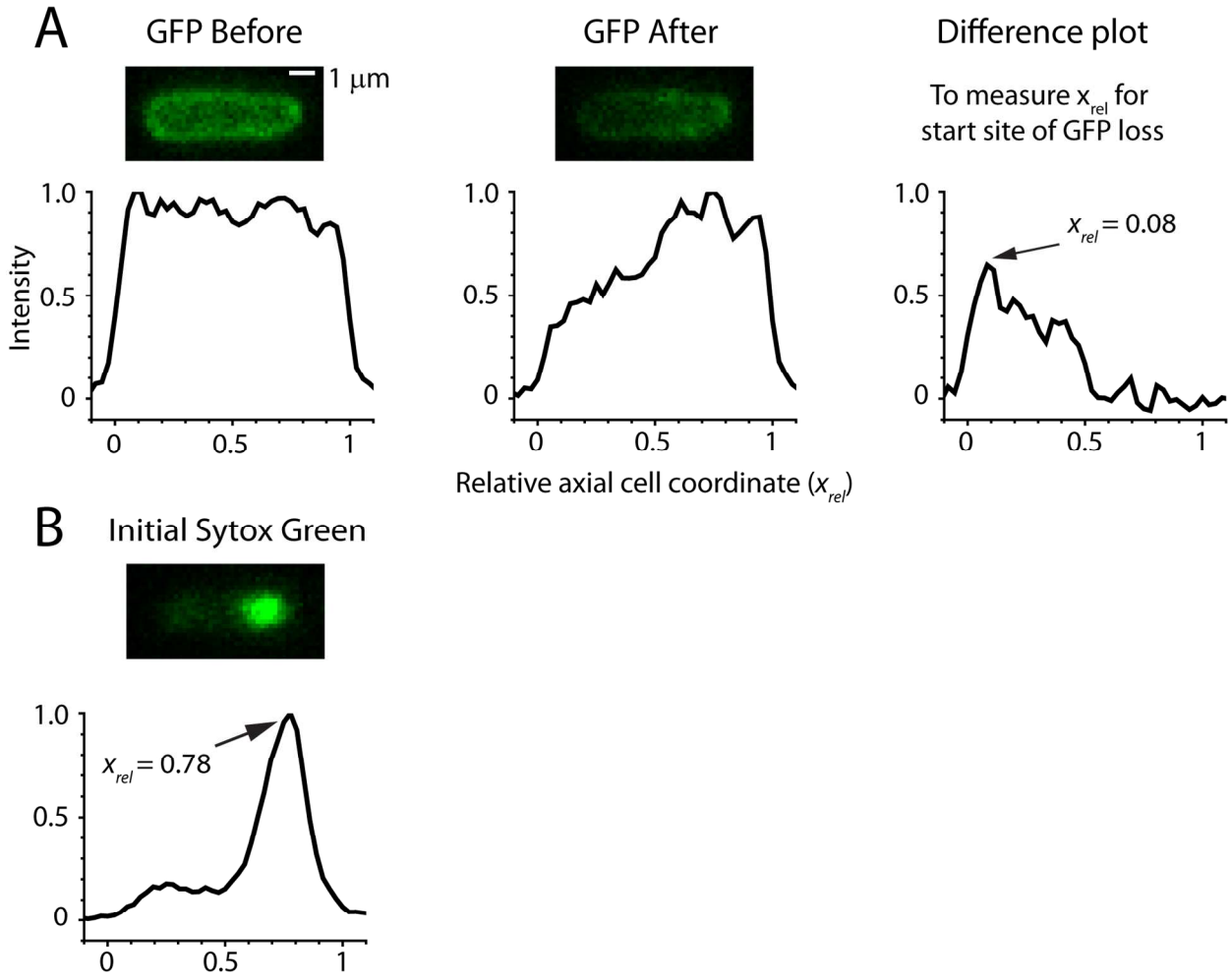

Figure S2. (A) Examples of axial linescans immediately before and after permeabilization of the OM and the difference plot. The axial location of the event is chosen at the intensity peak of the difference plot. (B) Axial linescan immediately after permeabilization of the CM. The axial

To estimate the axial location of the onset of GFP loss, we form the axial linescan for the cell image taken immediately after GFP loss begins (Fig. S2) and subtract the axial linescan of the "after" image from that of the "before" image. The difference linescan exhibits a local maximum corresponding to the distribution of the lost GFP (Fig. S2). The location of the onset of OM permeabilization was taken as the value of x_{rel} at the local maximum of the difference plot. Similarly, for the CM a cell image was chosen immediately after the appearance of the initial bright dot of Sytox Green fluorescence. The axial linescan for this image featured a peak, and the location of the onset of CM permeabilization was taken as the value of x_{rel} at the peak. See Figs. 8 and S11 for other examples.

Scatter plots for septating and non-septating cells (Fig. 3) were generated by plotting the location of OM permeabilization against the location of CM permeabilization for each cell that exhibited both behaviors clearly.

Additional histograms of timing and duration of permeabilization events

Figures S3, S4, and S5 present additional histograms of t_{OM}, t_{CM}, $(t_{CM} - t_{OM})$, Δt_{GFP}, and Δt_{Sytox} for the data at nominal 1 μM and 2 μM bulk Cecropin A concentration, obtained as described in the main text. Figure S3 combines both septating and non-septating cells, while Figs. S4 and S5 show data for septating cells alone and for non-septating cells alone. The lag time t_{OM} shows a substantial concentration dependence (see also 4 μM data in Table 1). The lag time $(t_{CM} - t_{OM})$ between OM and CM permeabilization is much less sensitive to concentration, as is also true for the GFP release time Δt_{GFP} and the Sytox Green entry time Δt_{Sytox}.

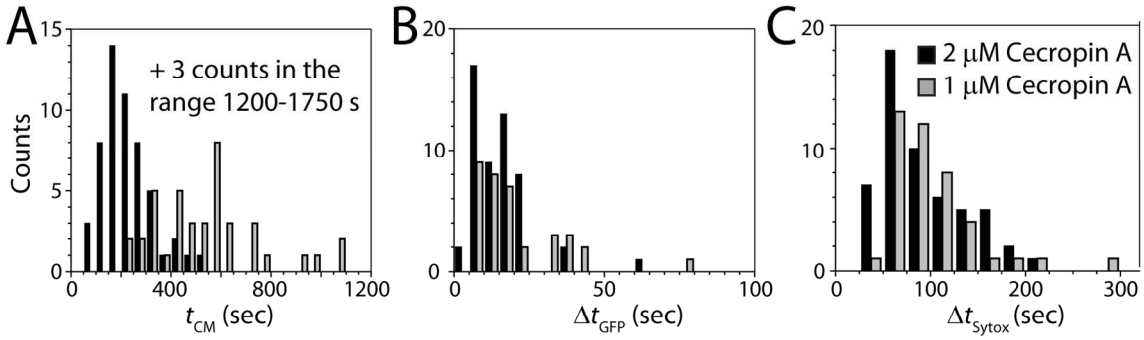

Figure S3. Histograms combining all cells, septating and non-septating, at 1 μM (grey bars) and 2 μM Cecropin A (black bars). See Fig. 5 of main text for t_{OM} and $(t_{CM} - t_{OM})$. **A.** Lag time to permeabilization of CM, t_{CM}. **B.** GFP release time, Δt_{GFP}. **C.** Sytox Green entry time, Δt_{Sytox}.

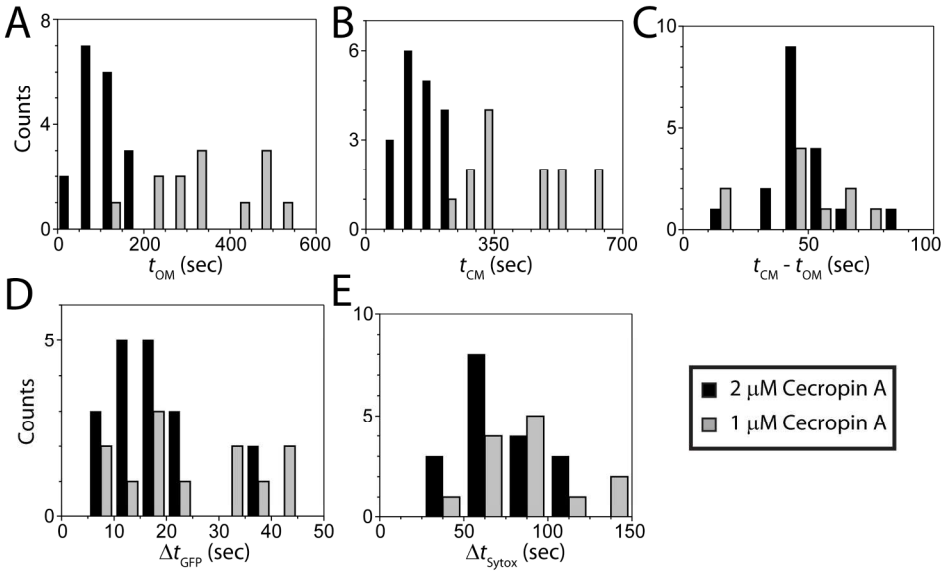

Figure S4. Histograms for septating cells only, at 1 μM (grey bars) and 2 μM Cecropin A (black bars). **A:** Lag time to permeabilization of OM, t_{OM}. **B:** Lag time to permeabilization of CM, t_{CM}. **C:** $(t_{CM} - t_{OM})$. **D:** GFP release time, Δt_{GFP}. **E:** Sytox Green entry time, Δt_{Sytox}.

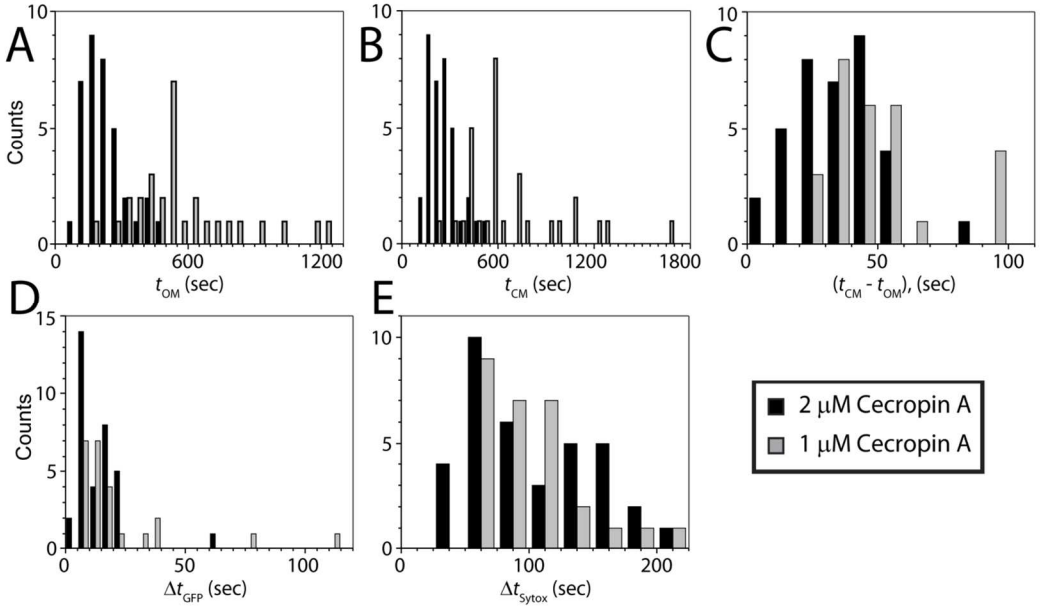

Figure S5. Histograms for non-septating cells only, at 1 μM (grey bars) and 2 μM Cecropin A (black bars). **A:** Lag time to permeabilization of OM, t_{OM}. **B:** Lag time to permeabilization of CM, t_{CM}. **C:** ($t_{CM} - t_{OM}$). **D:** GFP release time, Δt_{GFP}. **E:** Sytox Green entry time, Δt_{Sytox}.

Slowing of growth rate shortly after injection of Cecropin A

It is a subtle effect, but we sometimes observe a change in curvature of cell length vs time shortly after addition of Cecropin A and well before GFP exits and the cell shrinks. In exponential growth, $L(t)$ curves upward. In the plot in Fig. S6, $L(t)$ begins to curve downward for $t > 0$, the point of Cecropin A injection.

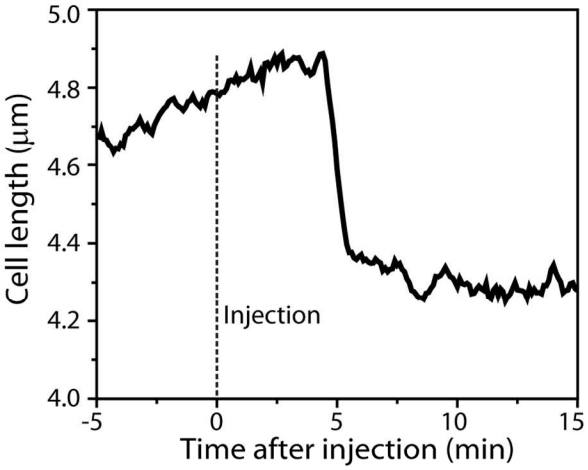

Figure S6. Decrease in growth rate shortly after injection of Cecropin A.

Monte Carlo simulations of GFP efflux from the periplasmic space

The periplasm is modeled as a thin, three-dimensional space sandwiched by two nested spherocylinders (Fig. 7A). The inner spherocylinder has a straight, cylindrical length L and endcap radius of R. The outer spherocylinder has the same cylindrical length of L, but the endcap radius is $(R + d)$, where d is the thickness of the model periplasmic space. The average tip-to-tip length of an *E. coli* cell in our growth conditions is ~5 μm. In earlier work under the same growth conditions, we measured the radius of *E. coli* cytoplasm to be 400 ± 25 nm.[1] Therefore, we fixed the values $L = 4.1$ μm and $R = 400$ nm. Cryo-transmission electron microscopy on frozen-hydrated sections of *E. coli* estimated the thickness of the periplasm to be ~ 20 nm.[2] The Monte Carlo step size must be small compared to the smallest dimensions, and simulations with such a small value of d were time consuming. We found that the value $d = 50$ nm shortens the computational time by 9X without significant effect on the timescale of the GFP release.

Initial positions for 20,000 particles were chosen randomly within the thin space. The diffusion coefficient D_{peri} was varied in the range 0.1-5.0 μm^2-s^{-1} to reach semi-quantitative agreement with the observed values of Δt_{GFP} (Table 1). Each particle step along the x, y, and z coordinates is chosen from a Gaussian distribution whose width is determined by D_{peri}. A particle is removed from the simulation whenever it crosses the absorbing surface patch. No "re-crossings" of the surface patch are permitted, meaning that the model yields the fastest possible drainage of GFP through a hole in the OM. In comparison, both a pore of finite thickness and a carpet patch would transmit GFP less efficiently. An example of a simulation trajectory eventually captured by a circular patch at the septum is shown in Fig. S7.

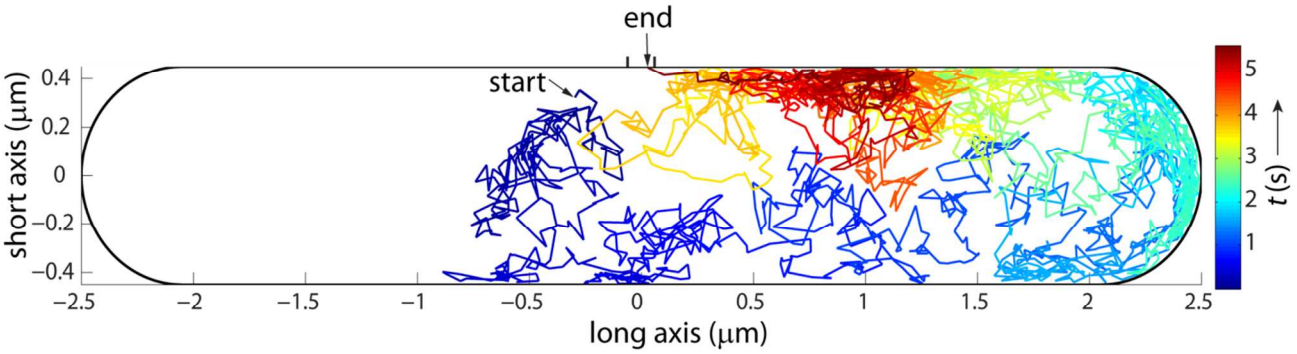

Figure S7. Diffusion to capture by a circular pore at the septum. Advancing time coded by color.

Figures S8 and S9 show the dependence of GFP loss curves on model geometry and on GFP diffusion coefficient for the absorbing annular ribbon at the septum and for a circular absorbing patch placed at one endcap. In Fig. S10, we compare experimental GFP loss from one non-septating cell with the model of a static, circular, absorbing endcap patch with parameter tuned to closely match Δt_{GFP}. The model decays more rapidly than experiment initially, and less rapidly than experiment later. From this we infer that the permeability of the cell is increasing in time.

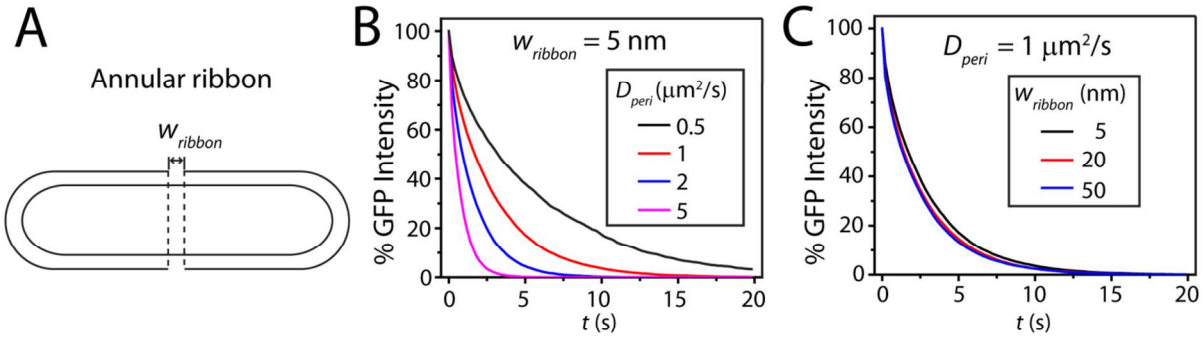

Figure S8. Monte Carlo simulations of GFP loss through an annular ribbon in the OM at the septum. **A**: Model geometry for the ribbon. **B**: Comparison of GFP intensity loss vs time with w_{ribbon} = 5 nm for different values of GFP diffusion constant D_{peri} as shown.
C: Comparison of GFP intensity loss vs time with D_{peri} = 1 μm^2-s^{-1} and different values of w_{ribbon} as shown. Narrow and wide ribbons capture molecules equally efficiently because whenever a molecule gets close to a ribbon, it has high probability of capture regardless of ribbon width.

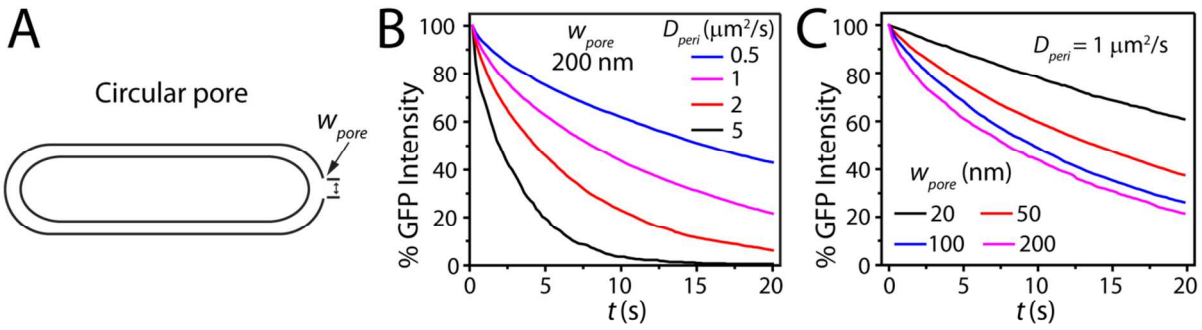

Figure S9. Monte Carlo simulations of GFP loss through a circular pore at the tip of the cell. **A**: Model geometry for a circular pore. **B**: Comparison of GFP intensity loss vs time with w_{pore} = 200 nm for different values of GFP diffusion constant D_{peri} as shown. **C**: Comparison of GFP intensity loss vs time with D_{peri} = 1 μm^2/s and different values of w_{pore} as shown.

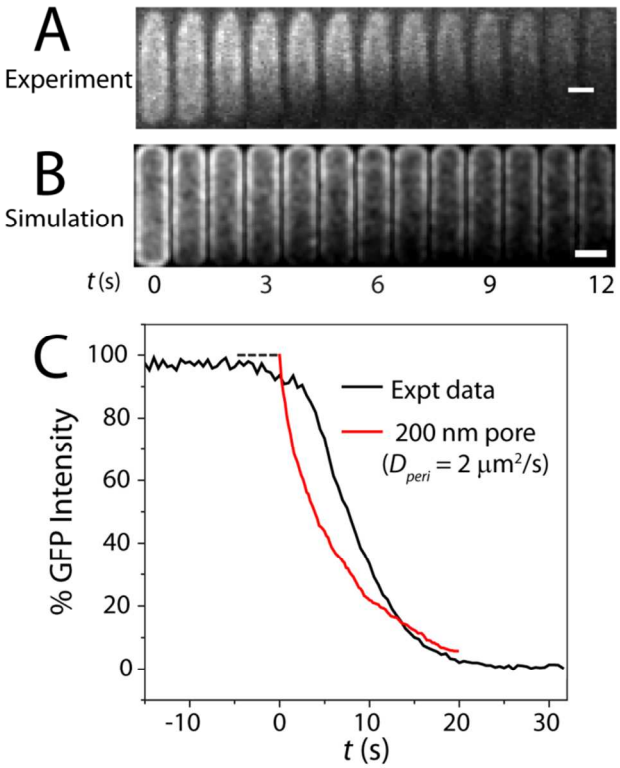

Figure S10. Two dimensional images of GFP loss from a non-septating cell. **A:** experimental example. **B:** Monte Carlo simulation using circular pore of 200 nm diameter and a diffusion constant D_{peri} = 2 μm^2/s. **C**: Comparison of GFP loss vs time for real cell and for the same model.

Comparison study of LL-37

Figure S11 illustrates the difference in the permeabilization behavior of LL-37 and Cecropin A in single septating cells. LL-37 permeabilizes both the OM and CM near the septum, at x_{rel} values of 0.52 and 0.58, respectively. Cecropin A permeabilizes the OM near the septum (x_{rel} = 0.56), but permeabilizes CM near an endcap (x_{rel} = 0.18).

A summary of the timing of events related to OM and CM permeabilization, GFP loss and Sytox Green staining is presented in Table S1.

Movie Example

Movie S1 shows the green fluorescence channel during the attack of Cecropin A on a representative septating cell (left panel) and non-septating cell (right panel), taken from the same field of view so that the time scale and Cecropin A concentrations match. Images were acquired at a rate of 1 frame every 0.6 s with exposure time of 50 ms/frame. Total imaging time was 6 min. The scale bar represents 1 μm. Images at the beginning of the movie corresponding to the periplasmic GFP signals were scaled 10X for both cells. The resulting movies were then autoscaled to maintain good visibility throughout.

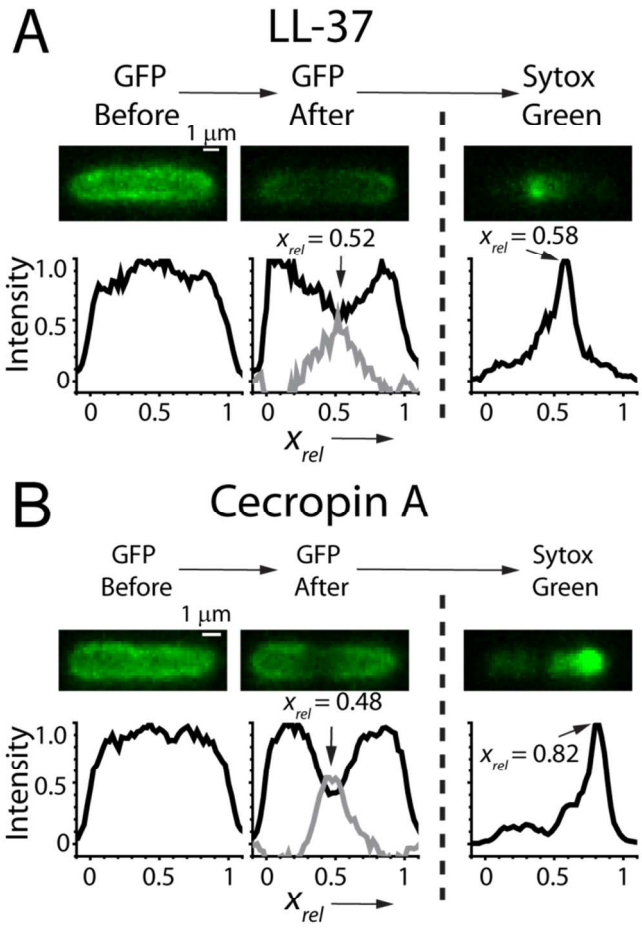

Figure S11: Axial intensity profiles of a single septating cell exposed to (**A**) LL-37 (4 μM) and (**B**) Cecropin A (2 μM). LL-37 permeabilizes both OM and CM near the septum. Cecropin A permeabilizes OM near septum and CM near an endcap. For (**A**) and (**B**), the two images and axial linescans at left were obtained just before and just after OM permeabilization to GFP. Subtraction of the two linescans makes the grey difference plot, from which we determine x_{rel} for the OM permeabilization event. The image and linescan at right shows the initial localized Sytox Green signal. We determine x_{rel} for CM permeabilization from the peak position of the axial linescan. See also Fig. S2.

Table S1. Summary of mean timing data for OM and CM permeabilization of *E. coli* by LL-37.

	Nominal Bulk Cecropin A Concentration	
	4 μM	**8 μM**
N_{tot} **(All cells)**	**9**	**19**
$\langle t_{OM} \rangle$	680 ± 540	220 ± 170
$\langle t_{CM} \rangle$	990 ± 330	350 ± 120
$\langle t_{CM} - t_{OM} \rangle$	320 ± 280	130 ± 150
$\langle \Delta t_{GFP} \rangle$	136 ± 89	60 ± 64
$\langle \Delta t_{Sytox} \rangle$	211 ± 93	89 ± 25
N_{sept} **(septating)**	**6**	**8**
$\langle t_{OM} \rangle$	262 ± 78	85 ± 43
$\langle t_{CM} \rangle$	916 ± 91	340 ± 120
$\langle t_{CM} - t_{OM} \rangle$	654 ± 78	250 ± 140
$\langle \Delta t_{GFP} \rangle$	130 ± 34	91 ± 54
$\langle \Delta t_{Sytox} \rangle$	220 ± 120	102 ± 25 (N = 8)
$N_{non\text{-}sept}$ **(non-septating)**	**3**	**11**
$\langle t_{OM} \rangle$	880 ± 560	310 ± 160
$\langle t_{CM} \rangle$	1030 ± 410	360 ± 130
$\langle t_{CM} - t_{OM} \rangle$	150 ± 160	50 ± 97
$\langle \Delta t_{GFP} \rangle$	140 ± 110	36 ± 63
$\langle \Delta t_{Sytox} \rangle$	205 ± 91 (N = 5)	76 ± 18

[a] All times in seconds. The ± values are one standard deviation of single measurements. *N* values give the number of cells in calculation of each mean.

References for Supporting Information

1. Bakshi, S., Bratton, B. P., and Weisshaar, J. C. (2011) Subdiffraction-limit study of Kaede diffusion and spatial distribution in live Escherichia coli, *Biophys J 101*, 2535-2544.

2. Matias, V. R., Al-Amoudi, A., Dubochet, J., and Beveridge, T. J. (2003) Cryo-transmission electron microscopy of frozen-hydrated sections of Escherichia coli and Pseudomonas aeruginosa, *J Bacteriol 185*, 6112-6118.